


Cite this: *RSC Adv.*, 2021, 11, 28452

Site-specific role of bifunctional graphitic carbon nitride catalyst for the sustainable synthesis of 3,3-spirocyclic oxindoles in aqueous media†

Anshu Dandia,^{*a} Dinesh Kumar Mahawar,^a Pratibha Saini,^a Surendra Saini,^a Shyam L. Gupta,^{ab} Kuldeep S. Rathore^c and Vijay Parewa^{id}^{*a}

Functionalized graphitic carbon nitride (Sg-C₃N₄) has been manufactured and used as a reusable catalyst for the one-pot production of various spiro-pyrano chromenes and spiro indole-3,1'-naphthalene tetracyclic systems in aqueous media. An ultrasound-assisted method has been used for the functionalization of g-C₃N₄. The catalytic functionalities and the structural integrity of the catalyst were characterized via different analytical tools. The catalytic site-specific role of Sg-C₃N₄ was confirmed via various control experiments in one-pot reaction sequences. We recognized that Sg-C₃N₄ acts as a bifunctional acid–base catalyst for the first reaction sequence whereas it is an acidic catalyst for the second reaction sequence during the one-pot production of various spiro-pyrano chromenes. In addition, the bifunctional acid–base catalytic role of Sg-C₃N₄ has been confirmed for the first reaction sequence whereas it has a basic catalytic role for the second reaction sequence during the one-pot production of spiro indole-3,1'-naphthalene tetracyclic systems. Diverse C–C, C–O, and C–N bonds, six-membered cycles, stereogenic centers, and spiro frameworks were formed in a single reaction, enhancing the biocidal profile and possibly resulting in the discovery of new medicinal properties. The mild reaction environment, simple workup, easy separation, low cost, heterogeneity, and recyclability of Sg-C₃N₄ are some rewards of this approach.

Received 18th May 2021
Accepted 8th August 2021

DOI: 10.1039/d1ra03881h

rsc.li/rsc-advances

1 Introduction

Carbon is one of the most multifaceted elements in the periodic table. Carbon-based substances have achieved insightful consequences in many areas of science and technology because of their noteworthy properties.¹ In previous decades, many scientists worked on developing inventive carbon-based compounds for wide-ranging applications.² Carbon materials have a splendid ability to provide at the nano-scale because they have fabulous thermal and electrical conductivity as well as lightness and elevated mechanical strength that traditional bulk substances cannot possess.³ With the multiplicity of their nanostructures, these distinctive values can be attained over an enormously broad range of environments. Therefore, they are exhaustively investigated for innumerable applications in optoelectronics and photonics, nanomedicine and

biotechnology, advanced electrodes and polymer composites.⁴ It is the chemical genius of carbon that it can create different nanostructures with entirely different properties.⁵ Amongst carbon-based substances, graphitic carbon nitride (g-C₃N₄), has elicited a huge focus in organic transformation because of its robust nature. g-C₃N₄ as an abundant and nontoxic substance can be effortlessly synthesized from carbon constituents, by the one-step polymerization of N-rich chemical compounds.⁶ Due to their distinctive properties they are potential candidates for a variety of applications in numerous fields.⁷ The significance of g-C₃N₄ as a catalyst or catalytic support has also been extensively recognized for numerous chemical reactions.⁸ However, the preparation of bifunctional g-C₃N₄ with acid and base sites is still a difficult task for the chemist. Enormous efforts⁹ have been made to introduce acidic groups into basic g-C₃N₄. But in these methods the inherent reasonable basic groups of g-C₃N₄ have been destroyed and the resulting material has very low or even no basicity. Therefore, there is a still a need for a mild and efficient protocol for the concurrent introduction of acid and base sites in g-C₃N₄ to make it a bifunctional catalyst.

Organic compounds with a spiro heterocyclic moiety are receiving wide scientific interest because of their distinctive conformational and chemical characteristics as well as the biological properties that are often coupled with the asymmetric spiro carbon atom.¹⁰ More specifically, the spiro-oxindole

^aCentre of Advanced Studies, Department of Chemistry, University of Rajasthan, Jaipur, India. E-mail: dranshudandia@yahoo.co.in; parewaviijay@uniraj.ac.in; parewaviijay.parewa@gmail.com

^bGovernment Polytechnic College, Near Itarana Fly Over, Kalimori, Ahwar, Rajasthan, 301001, India

^cDepartment of Physics, Arya College of Engineering and IT, Jaipur, India. E-mail: kuldeep_ssr@yahoo.com

† Electronic supplementary information (ESI) available. See DOI: 10.1039/d1ra03881h



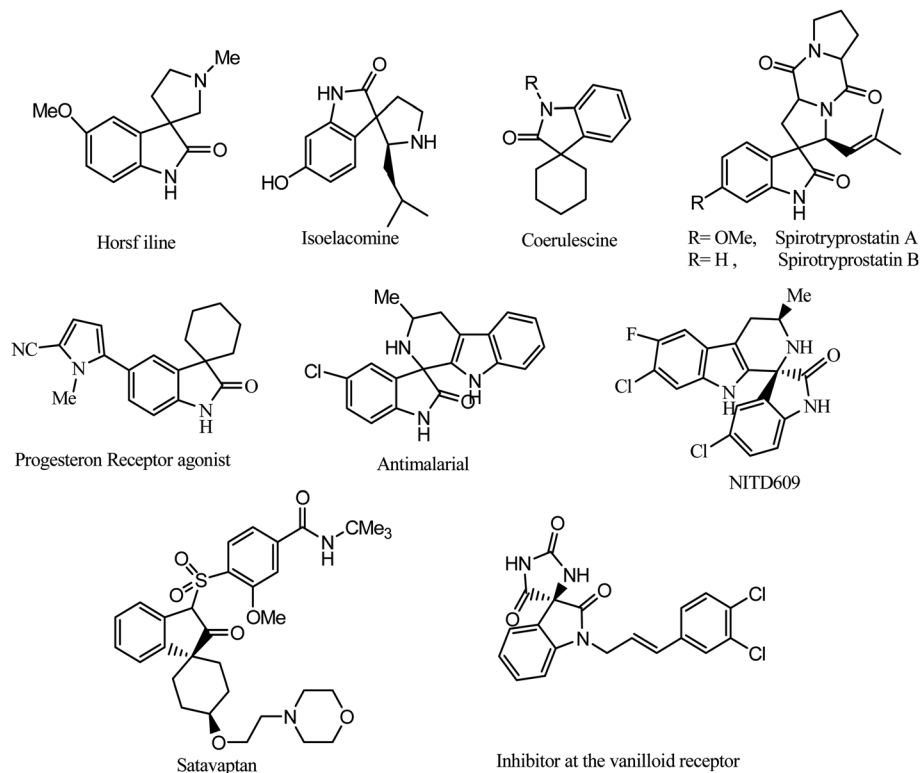
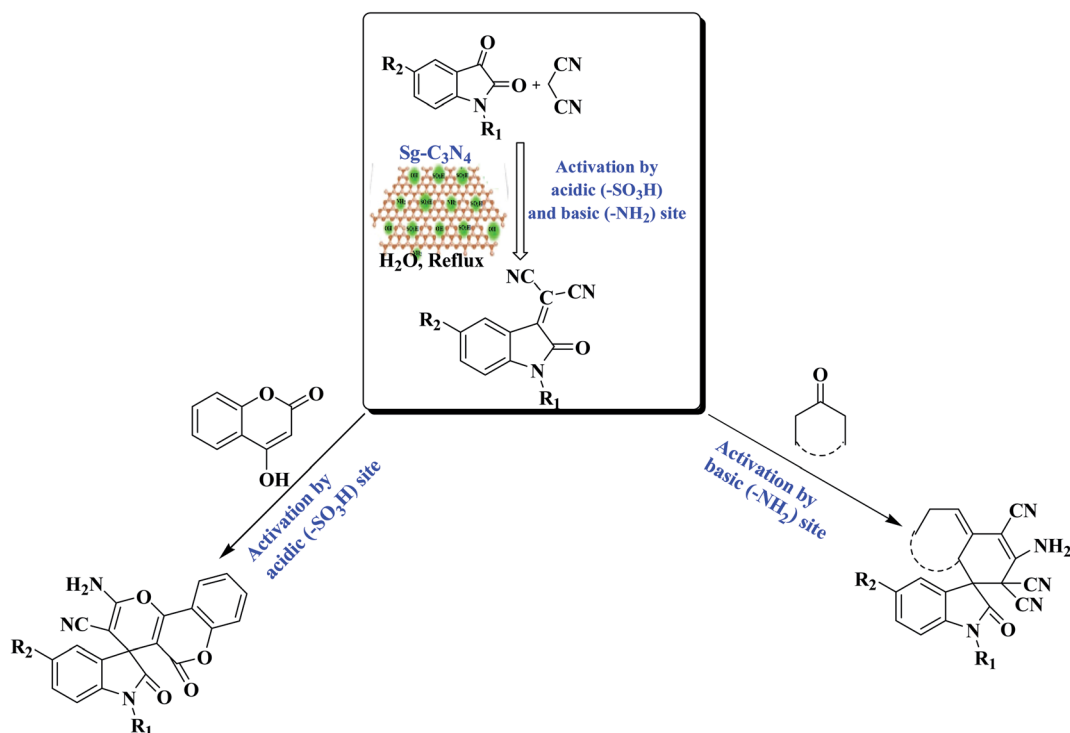


Fig. 1 Examples of spirocyclic oxindoles in natural products and pharmaceutical applications.

nucleus is found in a variety of biologically active heterocyclic compounds and natural products and can be of interest in the development of innovative clinically significant heterocyclic

motifs.¹¹ For example, a novel class of marine toxins isolated from dinoflagellates and shellfish, like pteriatxin and pinna-toxins,¹² shows that a spiro aza system is responsible for the



Scheme 1 The synthesis of various spiro-oxindole derivatives.

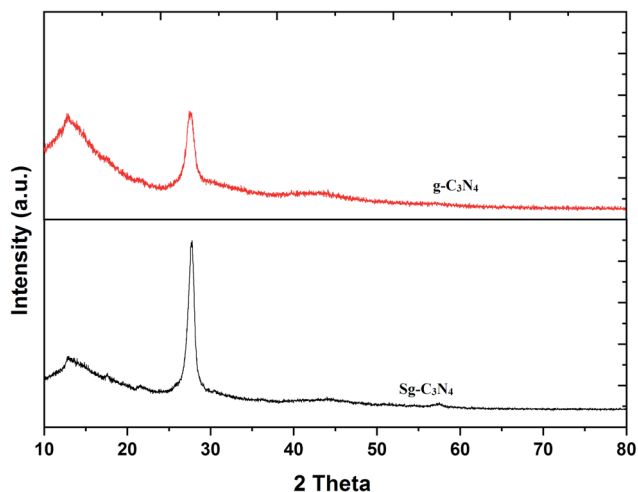


Fig. 2 XRD patterns of g-C₃N₄ and Sg-C₃N₄.

biological activity. Synthetic derivatives of spiro-oxindole ring systems, for example spirotryprostatin B, elacomine, alstonisine and horsfiline, have become imperative synthetic targets as

these structural frameworks form the central units of numerous naturally occurring compounds with important biological activities.¹³

Several spiro-oxindole derivatives show interesting biological activities (Fig. 1): for example, as progesterone receptor modulators,¹⁴ potent nonpeptide inhibitors of the p53-MDM2 interaction, and antitubercular,¹⁵ anticancer,¹⁶ anti-HIV,¹⁷ and antimalarial¹⁸ agents. Notably, the spiro-oxindole subunit is also found in spirotryprostatin A and B, which have been recognized as innovative inhibitors of microtubule assembly.¹⁹ In addition such spiro-oxindole heterocycles have been reported to be potent therapeutic agents against malaria. Isopteropodine and pteropodine have been found to modulate the utility of muscarinic serotonin receptors.²⁰

As a result of the extensive variety of the biological relevance of a 3,3-spirocyclic oxindole ring system with a quaternary center, enormous endeavors have been made to construct these bioactive spiro-oxindole derivatives by synthetic chemists. Numerous solvents and catalysts have been used to achieve this transformation.²¹ Recently, Shirini *et al.* described the synthesis

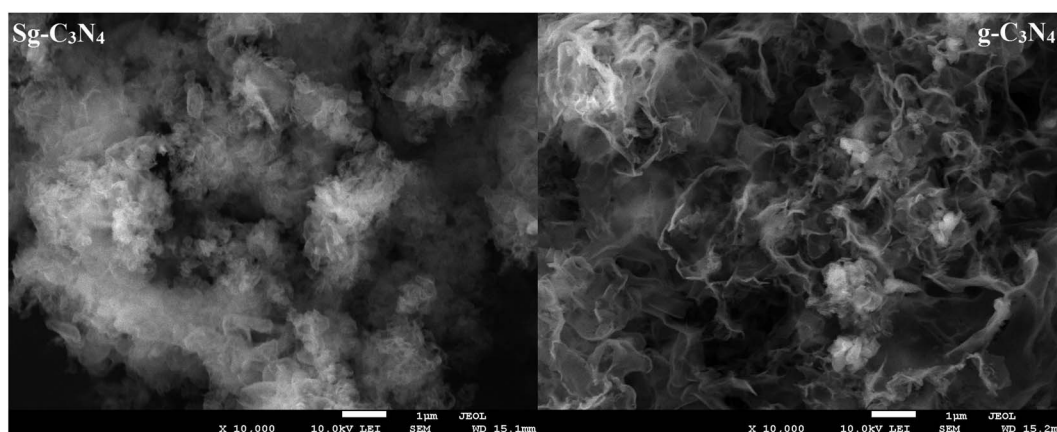


Fig. 3 SEM images of Sg-C₃N₄ and g-C₃N₄.

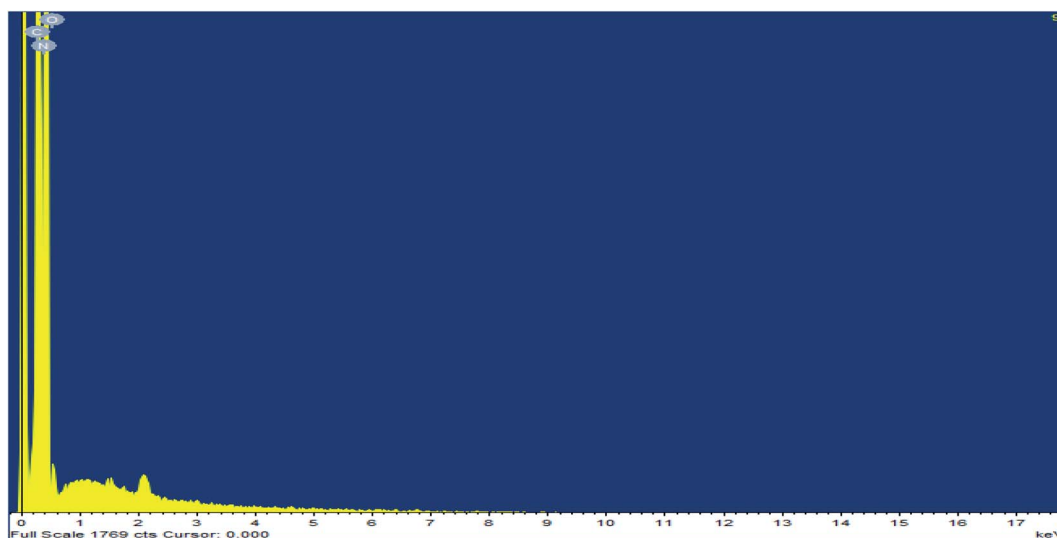


Fig. 4 EDAX analysis of g-C₃N₄.



of spiro-oxindoles using an $\text{Fe}_3\text{O}_4/\text{g-C}_3\text{N}_4$ nanocomposite.^{21k} Albeit with a subtle boost in reaction conditions, somewhere down the line they still fall short of the required flexibility. During our investigations on the synthesis of spiro derivatives and a detailed literature survey, it was observed that traditional methods suffer from many disadvantages: a multi-step process with a tedious workup procedure, prolonged refluxing in elevated harsh conditions using volatile or corrosive solvents and reactants with strong acidic/basic catalysts which may lead to the formation of the target product in lower yields. Furthermore, indigenous overheating can result in substrate, product or reagent decomposition, with a decrease in the yield of the required product, the formation of a mixture of products and a complicated isolation process with further purification using chromatographic techniques. Furthermore, the major shortcoming of nearly all current methods is that the catalysts are damaged in the workup process and cannot be recovered or recycled, reducing the turn over number (TON) or turn over frequency (TOF). In these environmentally conscious days, for reasons of economy and pollution, environ-economic green chemical procedures have to be developed to eliminate pollution problems, and replacing or reducing corrosive acids or volatile organic solvents in the reaction medium are among the most promising ways to reach these goals. Therefore, in an extension of our attempts towards the enlargement of novel synthetic methodologies for heterocyclic frameworks and nanoparticle synthesis,^{22,23} we have developed a bifunctional $\text{g-C}_3\text{N}_4$ (by the simultaneous incorporation of $-\text{SO}_3\text{H}$ and $-\text{NH}_2$ groups) by the reaction of melamine-derived $\text{g-C}_3\text{N}_4$ and aqueous H_2SO_4 under ultrasound irradiation. The bifunctional $\text{g-C}_3\text{N}_4$ ($\text{Sg-C}_3\text{N}_4$) has been characterized by diverse analytical techniques and used as a metal-free catalyst for the synthesis of various spiro-oxindole derivatives. Due to the admirable assistance between acid and base sites, the catalyst demonstrates a very high reactivity and selectivity for the synthesis of spiro-

oxindole derivatives. By comparable experiments, we have identified the responsible catalytic functionality in this $\text{Sg-C}_3\text{N}_4$ for the construction of various spiro-oxindole derivatives (Scheme 1).

2 Results and discussion

To achieve the goal of the convenient synthesis of bifunctional $\text{g-C}_3\text{N}_4$, we have firstly prepared pristine $\text{g-C}_3\text{N}_4$ from the easily available starting material melamine. Bifunctionalization of $\text{g-C}_3\text{N}_4$ has been accomplished by a simple ultrasound-assisted method through the reaction of pristine $\text{g-C}_3\text{N}_4$ and aqueous H_2SO_4 (30%). The as-prepared nanomaterials were characterized by XRD, SEM, EDAX, XPS and FT-IR analyses.

The crystal or amorphous structures and phase purity levels of the prepared $\text{g-C}_3\text{N}_4$ and $\text{Sg-C}_3\text{N}_4$ catalysts were investigated with X-ray diffraction (XRD) patterns (Fig. 2). There are two sharp diffraction peaks at 12.4° and 27.4° , corresponding to the (100) and (002) reflection of graphitic carbon of synthesized $\text{g-C}_3\text{N}_4$. The diffraction peaks of the XRD pattern of the synthesized $\text{Sg-C}_3\text{N}_4$ catalyst (H_2SO_4 -treated sample) are similar to those of the prepared catalyst $\text{g-C}_3\text{N}_4$. Despite the intensity of the (002) peak of $\text{Sg-C}_3\text{N}_4$ being higher with a minor change in its 2θ value compared to $\text{g-C}_3\text{N}_4$, this result indicates that the graphitic-like structures of the prepared catalyst still remained after the acid treatment. The extra exposed graphitic-like structural units of $\text{Sg-C}_3\text{N}_4$ are responsible for the increase in the intensity.

The micro-structures of $\text{g-C}_3\text{N}_4$, as revealed in the SEM images (Fig. 3) indicate the large aggregation of $\text{g-C}_3\text{N}_4$ units. The SEM image of the acid-treated sample ($\text{Sg-C}_3\text{N}_4$) reveals that there are no aggregations present in this sample because they are shattered into tiny particles with a more exposed and discrete surface, which is favorable for the strong interaction between the substance and the active acidic sites. The ordered

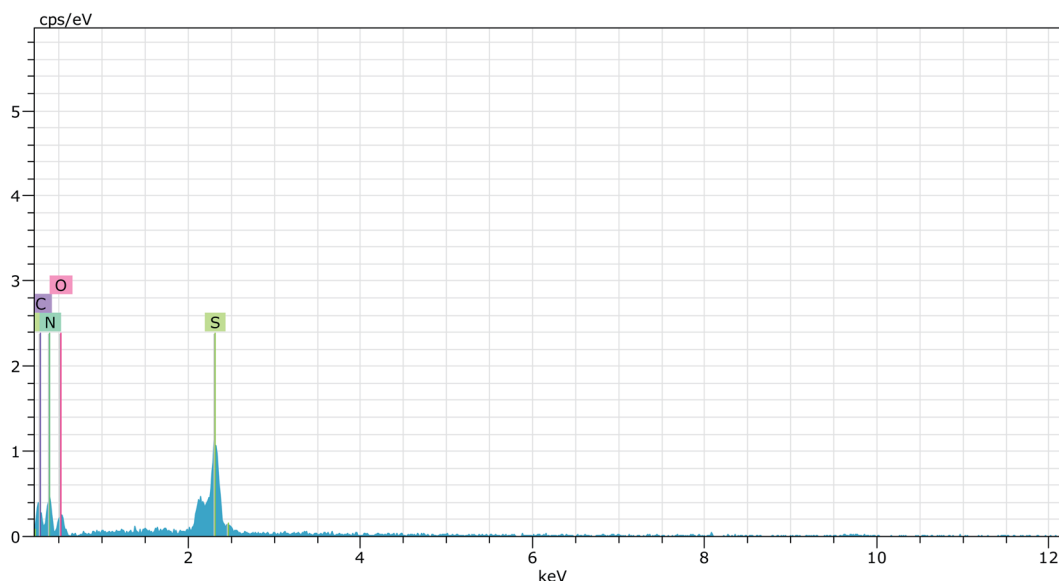


Fig. 5 EDAX analysis of $\text{Sg-C}_3\text{N}_4$.



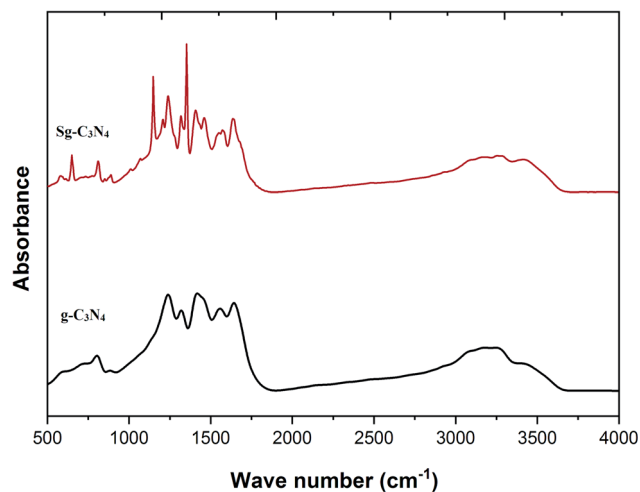


Fig. 6 FT-IR spectra of g-C₃N₄ and Sg-C₃N₄.

stacking of the CN layers was enhanced after H₂SO₄ treatment because H₂SO₄ treatment could exfoliate the g-C₃N₄ layers and generate more exposed g-C₃N₄ units.²⁴

Elemental analysis of simple graphitic carbon nitride achieved by EDAX analysis verifies the existence of C and N in g-

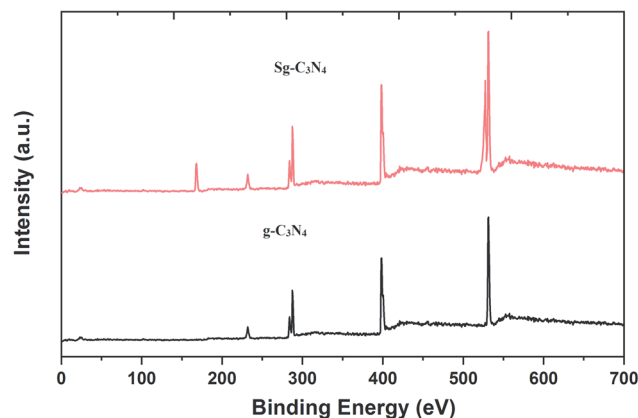


Fig. 8 XPS survey scans of g-C₃N₄ and Sg-C₃N₄.

C₃N₄ (Fig. 4 & 5). After acid treatment, the value of the carbon-nitrogen ratio reduces. Additionally, elemental analysis of the acid-treated sample (Sg-C₃N₄) verifies the existence of S, N, and C in the acid-treated sample. This proves that S was incorporated after the acid treatment. Similar results were also found in the elemental analysis (CNOS) of the samples (Table S1†).

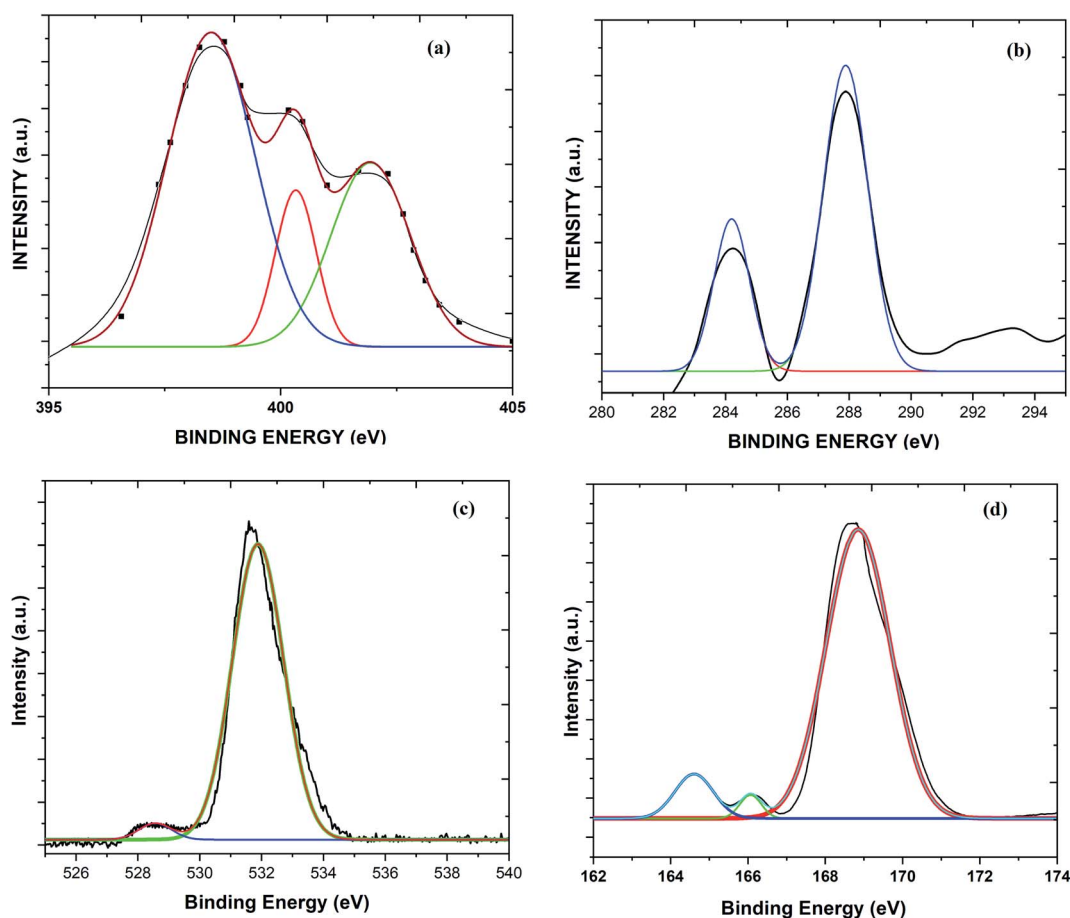
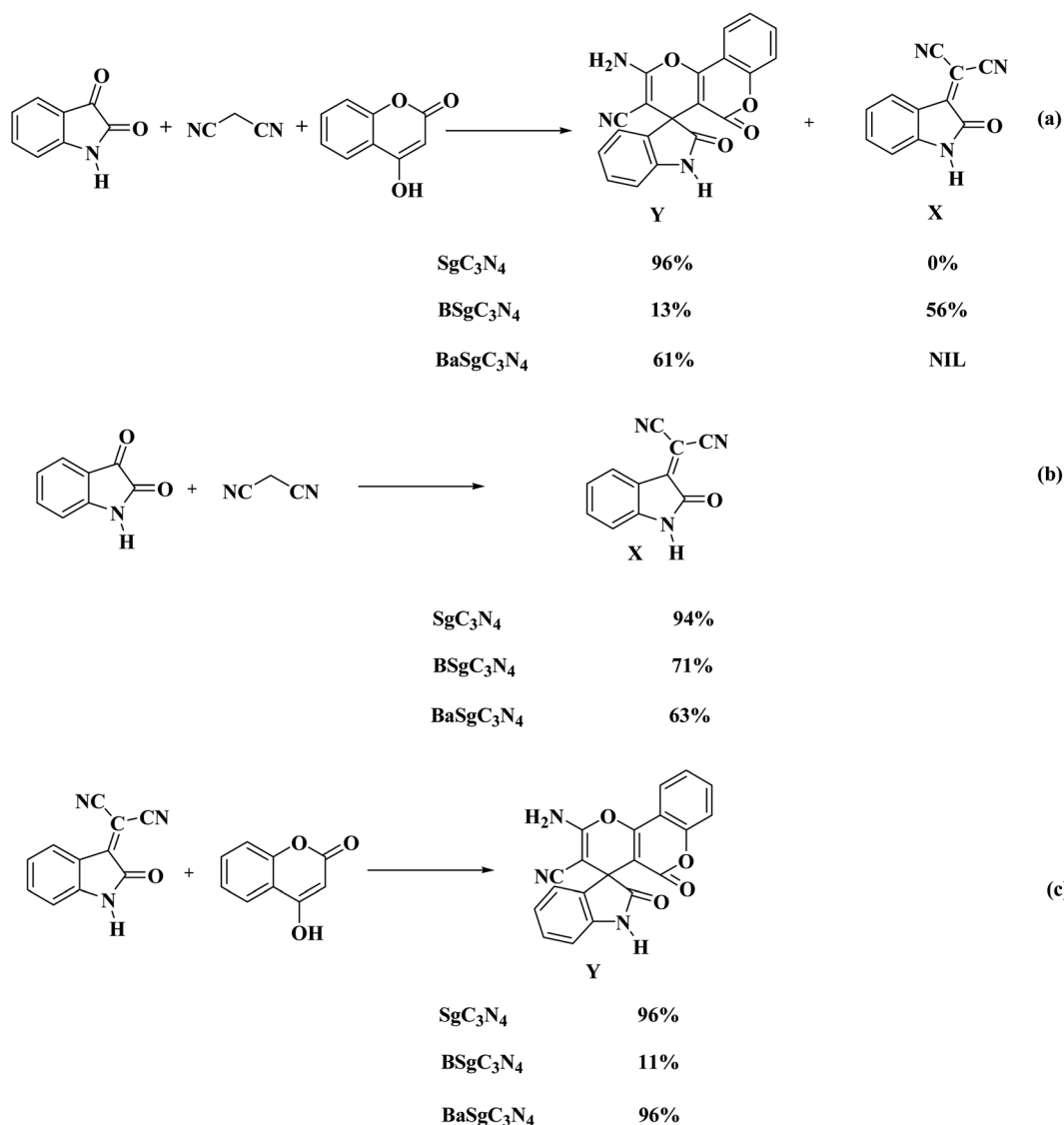


Fig. 7 XPS spectra: (a) the N 1s spectrum of Sg-C₃N₄, (b) the C 1s spectrum of Sg-C₃N₄, (c) the O 1s spectrum of Sg-C₃N₄, and the (d) S 2p spectrum of Sg-C₃N₄.



Table 1 Optimization of the reaction conditions for the production of spiro-pyrano chromen (**4a**)^a

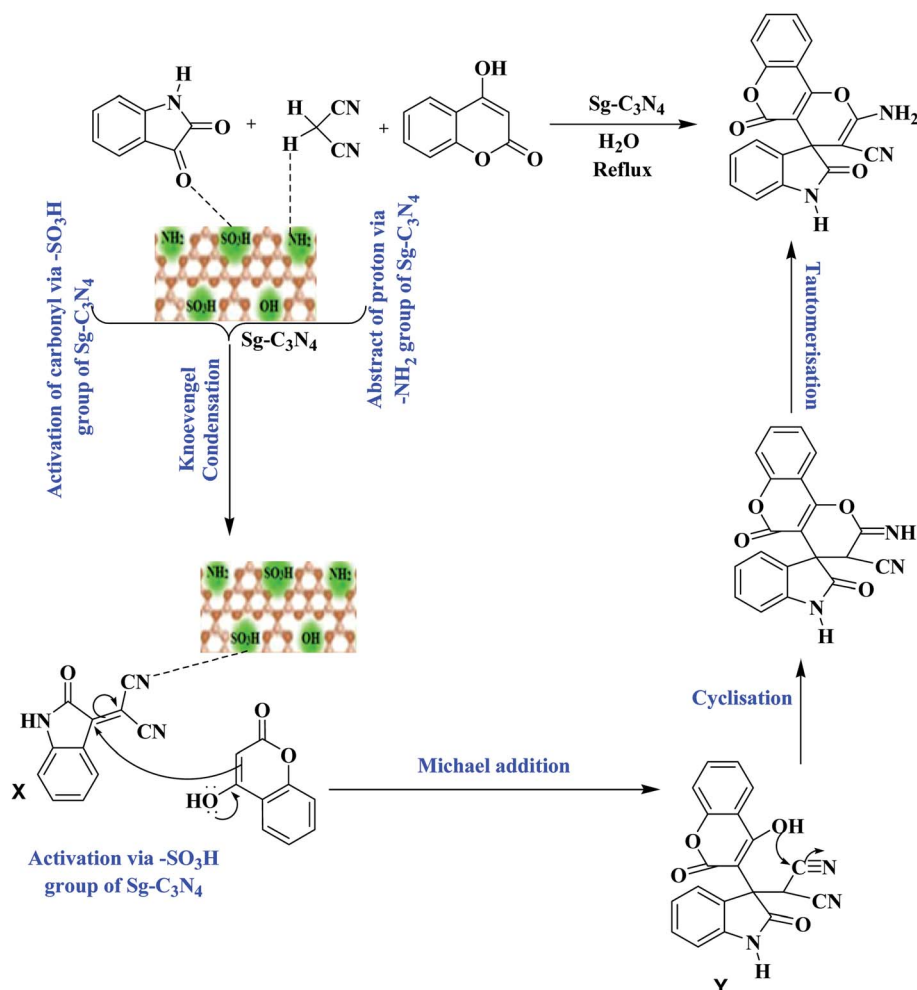
S. No.	Catalyst	Solvent	Time (min)	Yield ^b (%)	TOF ^c
1	—	H ₂ O	5 h	42	n.c.
2	I ₂ (20 wt%)	H ₂ O	60	52	0.092
3	PTSA (20 wt%)	H ₂ O	60	59	0.105
4	MWCNTs (20 wt%)	H ₂ O	60	28	0.050
5	Graphite (20 wt%) ^d	H ₂ O	60	—	—
6	Activated carbon (20 wt%)	H ₂ O	60	14	0.025
7	GO (20 wt%)	H ₂ O	60	43	0.076
8	rGO (20 wt%)	H ₂ O	60	20	0.035
9	g-C ₃ N ₄ (20 wt%)	H ₂ O	10	34	0.363
10	Sg-C ₃ N ₄ (20 wt%)	H ₂ O	10	96	1.024
11	Sg-C ₃ N ₄ (10 wt%)	H ₂ O	20	57	0.686
12	Sg-C ₃ N ₄ (30 wt%)	H ₂ O	10	96	0.598
13	Sg-C ₃ N ₄ (20 wt%)	CH ₃ CN	30	28	0.099
14	Sg-C ₃ N ₄ (20 wt%)	EtOH	30	17	0.060
15	Sg-C ₃ N ₄ (20 wt%)	THF	30	39	0.139
16	Sg-C ₃ N ₄ (20 wt%)	CH ₂ Cl ₂	30	36	0.128

^a All reactions were performed with isatin (2.0 mmol), malononitrile (2.0 mmol), and 4-hydroxycoumarin (2.0 mmol) under reflux. ^b Isolated yield.^c TOF ($\times 10^{-3}$ mol g⁻¹ min⁻¹). ^d Multi-walled carbon nanotubes.**Scheme 2** Various control experiments for the synthesis of spiro-pyrano chromen.

FT-IR spectra of the prepared carbon nitride materials $g\text{-C}_3\text{N}_4$ and $\text{Sg-C}_3\text{N}_4$ are presented in Fig. 6. The sharp band at 808 cm^{-1} is assigned to the tris-*s*-triazine layers of the synthesized samples. Broad peaks at around $3040\text{--}3380\text{ cm}^{-1}$ are instigated by the N-H vibration modes for -NH_2 groups. An absorption band at 1635 cm^{-1} corresponds to the typical stretching modes of CN heterocycles. A range of bands in the region of $1462\text{--}1570\text{ cm}^{-1}$ can be related to the tris-*s*-triazine of the melamine constituent. A signal at 1407 cm^{-1} is equivalent to the stretching vibrations of C-N bonds in tertiary N-atoms in the units of the prepared catalyst. Various bands in the range of $1209\text{--}1314\text{ cm}^{-1}$ correspond to sp^2 hybridized C-(NH) entities. After the acid treatment, a sharp band at 649 cm^{-1} is attributed to the presence of $\text{-SO}_3\text{H}$ functionality in the $\text{Sg-C}_3\text{N}_4$ catalyst. The appearance of two strong peaks at 1352 and 1148 cm^{-1} (because of asymmetric and symmetric stretching vibrations) also confirms the occurrence of an $\text{-SO}_3\text{H}$ group. The broad peaks at around $3000\text{--}3400\text{ cm}^{-1}$ are instigated by free amino and hydroxyl functionalities. These results confirm that acid-treated samples initiate several new functional groups (NH_2 & SO_3H) in the carbon nitride nanosheet.

The occurrence of different surface atoms (chemical environment) and oxidation states in the prepared $g\text{-C}_3\text{N}_4$ and $\text{Sg-C}_3\text{N}_4$ catalysts were examined using the X-ray photoelectron spectroscopic (XPS) method (Fig. 7, and S3†). The XPS deconvoluted C 1s spectra of the samples show two characteristic peaks with binding energies of 288.2 and 284.4 eV owing to the occurrence of sp^2 -hybridized C elements in the prepared samples. The three peaks at 397.7 , 399.2 and 400.3 eV in the N 1s spectrum of the samples belong to N element (sp^2 -bonded), tertiary N element and primary N element, respectively. The two peaks in the O 1s spectra of the samples with binding energies of 530.6 eV and 528.7 eV correspond to -OH functional groups. On the other hand, a study of the XPS survey spectrum of $g\text{-C}_3\text{N}_4$ with $\text{Sg-C}_3\text{N}_4$ reveals that intensity of the C 1s spectrum is reduced while the intensity of the N 1s and O 1s spectra is enhanced. A peak at around 232 eV in both survey spectra may arise due to the Auger spectra of C KLL.²⁵

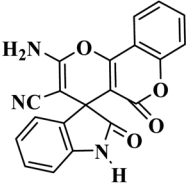
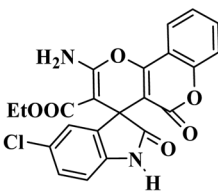
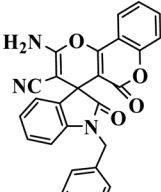
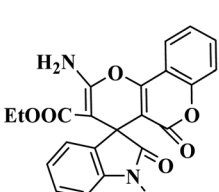
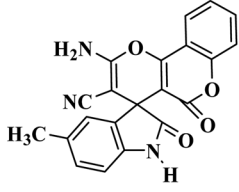
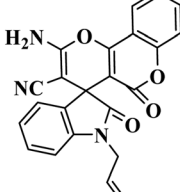
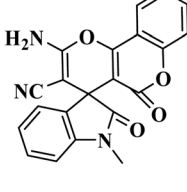
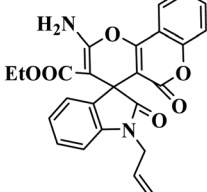
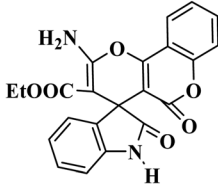
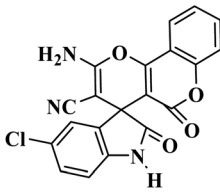
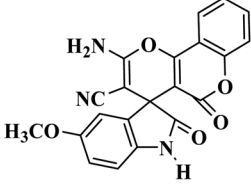
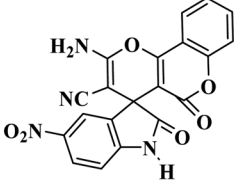
The XPS survey spectrum in Fig. 8 demonstrates the occurrence of C, N, O atoms in a simple carbon nitride sample, whereas the XPS spectrum of the $\text{Sg-C}_3\text{N}_4$ sample has C, N, S and O species without other impurities. XPS analysis of the elemental S 2p spectrum of $\text{Sg-C}_3\text{N}_4$ allocates three peaks with



Scheme 3 The probable mechanistic pathway for the production of spiro-pyrano chromens.



Table 2 Synthesis of spiro-pyrano chromens^a

 4a; 10 min.; 96%	 4b; 8 min.; 94%	 4c; 10 min.; 90%	 4d; 12 min.; 95%
 4e; 8 min.; 93%	 4f; 9 min.; 88%	 4g; 10 min.; 92%	 4h; 12 min.; 89%
 4i; 8 min.; 93%	 4j; 10 min.; 95%	 4k; 12 min.; 92%	 4l; 10 min.; 91%

^a All reactions were performed with substituted isatins (2.0 mmol), malononitrile/ethyl cyanoacetate (2.0 mmol), and 4-hydroxycoumarin (2.0 mmol) using 20 wt% Sg-C₃N₄ in water and were completed in 30 to 45 min.

binding energies of 164.0 eV (C-S bond), 165.8 eV (-N-S bond) and 169.1 eV (-N-S bond). Furthermore, the characteristic peak at 169.1 eV is ascribed to the -S=O group in Sg-C₃N₄, which further verifies the existence of -SO₃H functionalities in the prepared Sg-C₃N₄ sample. FT-IR and X-ray photoelectron spectroscopy examinations verify the healthy incorporation of SO₃H and NH₂ functionalities into g-C₃N₄ after acid treatment.

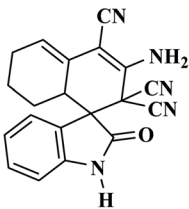
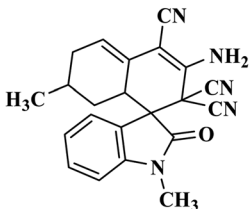
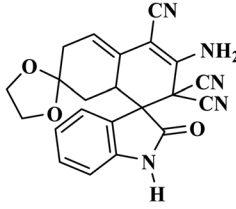
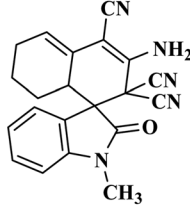
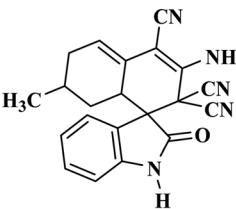
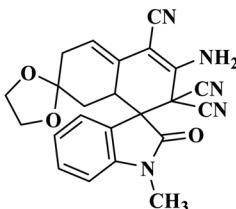
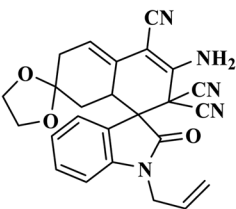
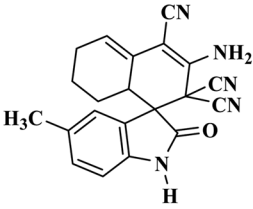
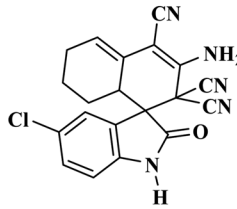
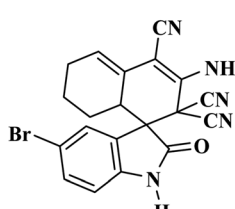
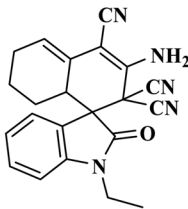
After the identification of the fundamental nature of the samples, we assessed the catalytic activity of these sample towards the synthesis of spiro-oxindoles. Our preliminary attempts concentrated on optimization of the production of spiro-pyrano chromen derivatives. The reaction of isatin **1** (2.0 mmol), malononitrile **2** (2.0 mmol) and 4-hydroxycoumarin **3** (2.0 mmol) was selected as a model reaction. Without any catalyst a lower yield of the product was formed. To enhance the efficacy of the protocol, different metal-free materials were screened as catalysts. As mentioned in Table 1, the most appealing outcome was obtained with Sg-C₃N₄ as the catalyst in terms of turnover frequency (TOF) compared to other catalysts. It was found that 20 wt% Sg-C₃N₄ in H₂O is enough to drive the reaction forward. Any excess of Sg-C₃N₄ beyond this amount did not show any further increase in yield. g-C₃N did not show any significant impact on the reaction, which demonstrates that

acid treatment generated functionality plays a vital role in the reaction.

To confirm which functionality in Sg-C₃N₄ plays a vital role in the reaction, Sg-C₃N₄ was employed in basic conditions (refluxed with NaOH and NaCl) to acquire base-treated Sg-C₃N₄ (BSg-C₃N₄). The FT-IR intensity of the -SO₃H group in BSg-C₃N₄ was relatively weak because of the deprotonation of the -SO₃H group (Fig. S1; see ESI[†]). The intensity of the FT-IR band due to the sp²-C mode was improved because of the additional room in the π-π* network caused by the dehydration reaction forced by the base. The FT-IR band of -NH₂ groups is stable in basic conditions so this intensity remains unchanged. This BSg-C₃N₄ was further converted into BaSg-C₃N₄ by acidic treatment with 0.1 M HCl. The FT-IR intensity of the -SO₃H group can be restored because of reprotonation of the -SO₃H group (Fig. S2; see ESI[†]). But the intensity of the FT-IR band due to -NH₂ groups could not be restored due to the neutralization of basic groups by the acid treatment.

To investigate the mechanism for the catalytic action of the catalyst, some control trials were executed using BSg-C₃N₄ and BaSg-C₃N₄ catalysts (Scheme 2). When the model reaction was tried with BSg-C₃N₄, isatylidene malononitrile (**X**) was isolated as a major product instead of spiro-pyrano chromen. While

Table 3 Synthesis of spiro indole-3,1'-naphthalene tetracyclic systems^a

			
6a; 12 min.; 95%	6b; 12 min.; 94%	6c; 15 min.; 92%	6d; 12 min.; 93%
			
6e; 12 min.; 92%	6f; 15 min.; 91%	6g; 15 min.; 89%	6h; 10 min.; 92%
			
6i; 12 min.; 93%	6j; 15 min.; 92%	6k; 10 min.; 91%	

^a All reactions were performed with substituted isatins (2.0 mmol), malononitrile (4.0 mmol), and cyclic ketones (2.0 mmol) using 20 wt% Sg-C₃N₄ in water and were completed in 30 to 45 min.

BaSg-C₃N₄ confirmed substantial recovery in catalytic activity for the selective synthesis of spiro-pyrano chromen. However an excellent yield of spiro-pyrano chromen was observed with Sg-C₃N₄. No side product was formed under these conditions (Scheme 2a).

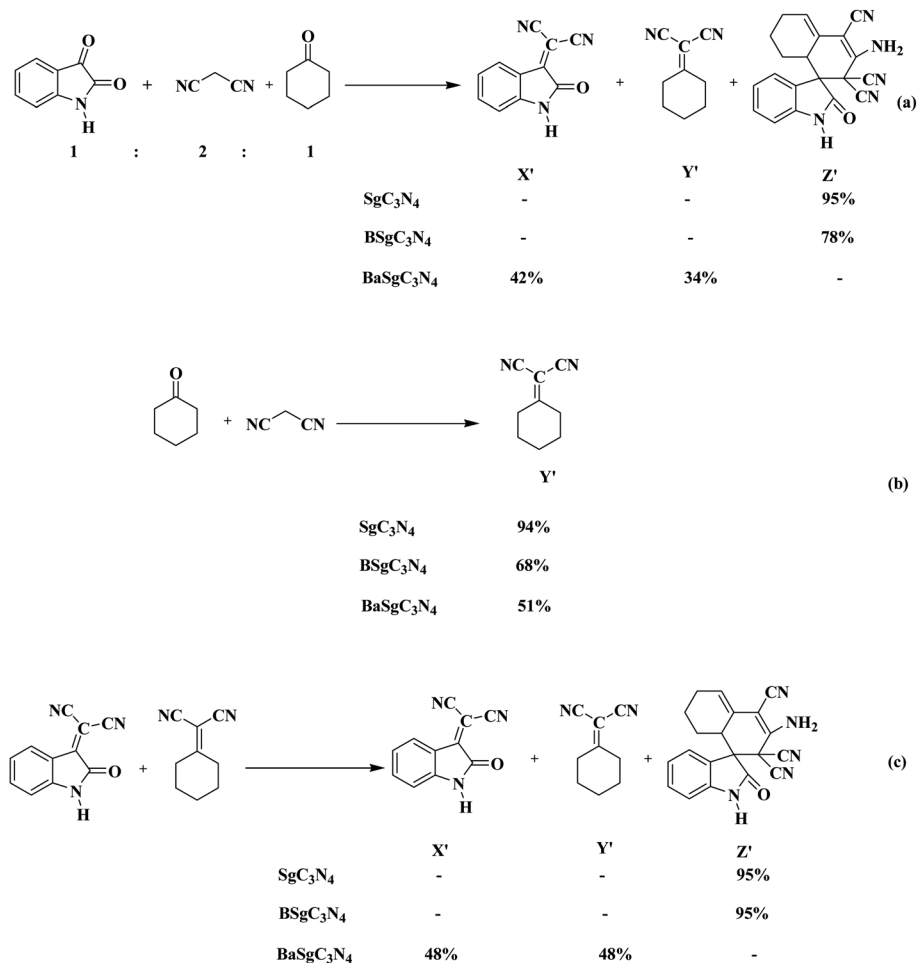
To further confirm the site-specific role of this bifunctional catalyst, we carried out the stepwise synthesis of the desired product under control conditions. When the reaction of isatins with malononitrile was run with Sg-C₃N₄, corresponding Knoevenagel adducts were produced in excellent yield. While moderate yields were observed with BSg-C₃N₄ and BaSg-C₃N₄ catalysts (Scheme 2b). This outcome confirms the vital role of the -SO₃H group and -NH₂ groups for the formation of an Knoevenagel adduct. Moreover, we prepared the Knoevenagel adduct and subjected this adduct with 4-hydroxycoumarin to the control conditions. Sg-C₃N₄ was found to be the best catalyst for the synthesis of the desired product. BSg-C₃N₄ gave an inferior yield of the product. Significant improvement in catalytic activity was detected with BaSg-C₃N₄ (Scheme 2c). These experiments illustrate that -SO₃H groups are the sites in Sg-C₃N₄ responsible for the above transformation.

Thus, these reaction profile indicates that the sites responsible for the Knoevenagel reaction are the -SO₃H group and -NH₂ groups and a further attack on 4-hydroxycoumarin was facilitated by the -SO₃H groups of the Sg-C₃N₄ catalyst in a one-pot process.

Various solvents (like ethanol, CH₃CN, THF, DCM and H₂O) were also tested on the model reaction. The outcomes suggested that the solvents had a remarkable impact on the product yield. The best transformation was noticed when the conversion was carried out in water. g-C₃N₄ treated with 30% aqueous H₂SO₄ demonstrates the highest yield of the product among the different examined concentrations (10%, 20%, 30% and 40%).

Based on these outcomes, a probable mechanistic pathway for the synthesis of spiro-pyrano chromen is presented in Scheme 3. Firstly, Sg-C₃N₄ acts as a bifunctional catalyst and activates isatins and malononitrile for the Knoevenagel reaction and produces isatylidene malononitrile (X). Afterwards, the -SO₃H group of Sg-C₃N₄ facilitates Michael addition and forms intermediate Y. Subsequent cyclization of intermediate Y followed by tautomerization produces desired product 3a.





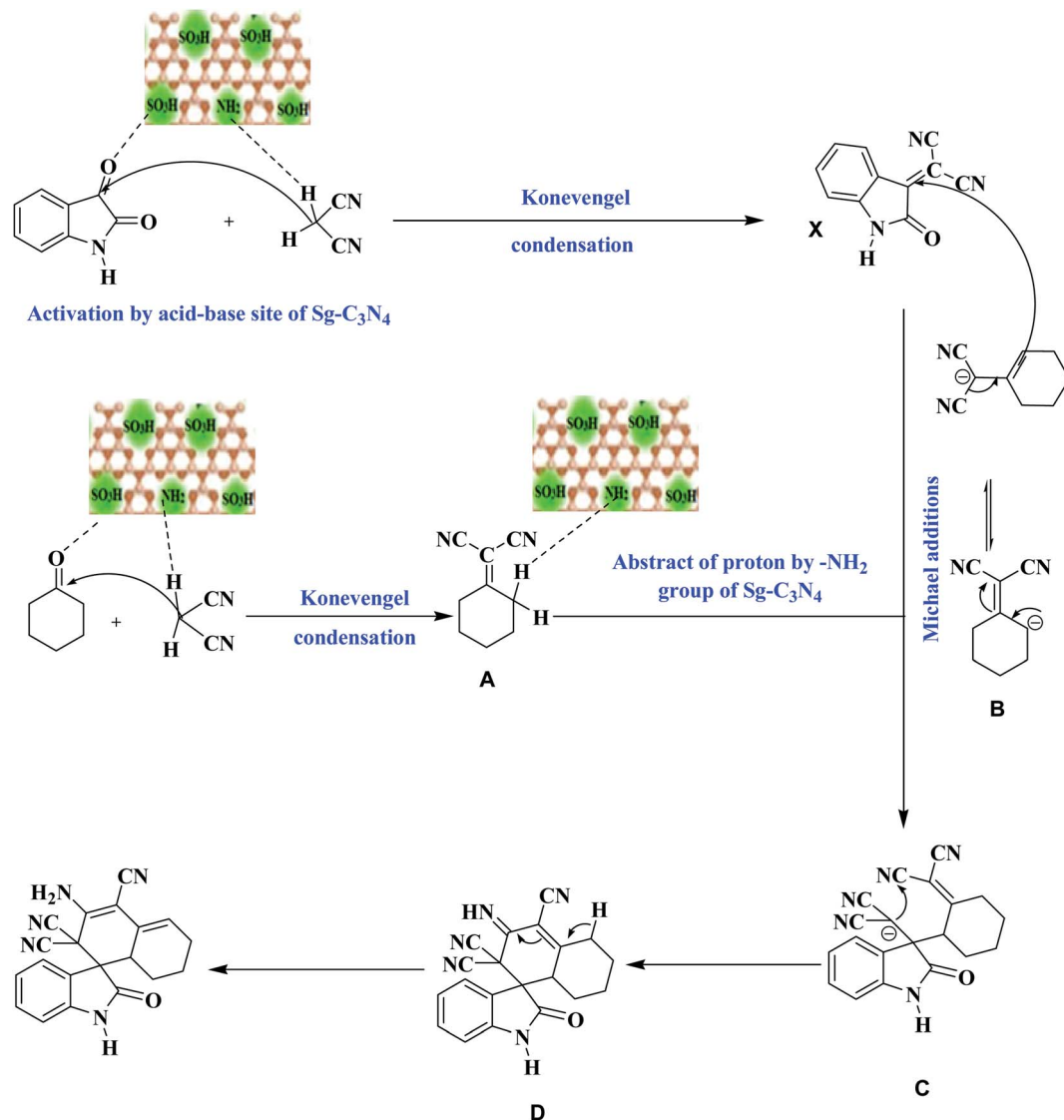
Scheme 4 Various control experiments for the synthesis of a spiro indole-3,1'-naphthalene tetracyclic system (a–c).

To demonstrate the scope and versatility of this methodology under identical reaction conditions, a library of substituted medicinally relevant spiro-pyrano chromens was produced (Table 2). Isatins with different electron donating and withdrawing groups on the aromatic ring do not influence the reaction profile that much and give the desired product in excellent yield. N-substituted isatins also tolerate the reaction conditions and produce the desired product in good to excellent yield. The same one-pot method also proceeded efficiently with ethyl cyanoacetate in place of malononitrile. No noteworthy deviation in yields of the products was detected in the case of ethyl cyanoacetate. The conversion completes well and the desired compounds are isolated in good yields.

Encouraged by these results, we broadened the scope of the above approach for the production of other types of pharmaceutically imperative spiro indole-3,1'-naphthalene tetracyclic systems.²⁶ According to the literature, synthesis of these compounds requires the previous production of Knoevenagel adducts, which involves two extra steps in the synthesis of target compounds.²⁷ We have effectively applied the above optimized conditions for the production of these systems by a one-pot process using isatins, malononitrile and cyclohexanone in a 1 : 2 : 1 ratio. Various substituted isatins tolerated the

reaction conditions and formed the corresponding functionalized spiro-oxindoles in excellent yield. The reaction also proceeded proficiently under similar experimental conditions with other types of cyclic ketones (Table 3).

We have also done some control experiments to confirm which catalytic site in Sg-C₃N₄ was responsible for the above conversion (Scheme 4). To accomplish the appropriate conditions to afford the spiro indole-3,1'-naphthalene tetracyclic system, a model reaction was performed between isatin, malononitrile and cyclohexanone under control conditions using, Sg-C₃N₄, BSg-C₃N₄ and BaSg-C₃N₄ catalysts (Scheme 4a). An admirable yield of the product was viewed with Sg-C₃N₄. No side product was produced under these conditions. Selective synthesis of a spiro indole-3,1'-naphthalene tetracyclic system was also observed with BSg-C₃N₄, but the yield of the product was lower compared to Sg-C₃N₄. While with BaSg-C₃N₄, Knoevenagel adducts were formed instead of a spiro indole-3,1'-naphthalene tetracyclic system. We have already established the bifunctional role of Sg-C₃N₄ for the synthesis of isatylidene malononitrile (Scheme 2b). Analogous results were found for the formation of cyclohexanone malononitrile (Scheme 4b). Moreover, we also carried out the reaction of isatylidene malononitrile and cyclohexanone malononitrile with Sg-C₃N₄, BSg-



Scheme 5 A probable mechanistic pathway for the synthesis of a spiro indole-3,1'-naphthalene tetracyclic system.

C₃N₄ and BaSg-C₃N₄ catalysts (Scheme 4c). Sg-C₃N₄ produced the desired product in excellent yield. BSg-C₃N₄ also acts as an active catalyst for the above transformation, but the yield of the product was lower compared to Sg-C₃N₄. A substantial loss in catalytic activity was observed when the reaction was tried with BaSg-C₃N₄. The desired product was not formed and the reactants remained unchanged under these conditions.

Hence, these results illustrate that the sites responsible for the Knoevenagel reaction are the -SO₃H group and -NH₂ groups, and furthermore the reaction of isatylidene malononitrile and cyclohexanone malononitrile was encouraged by the -NH₂ groups of the Sg-C₃N₄ catalyst in a one-pot process.

Based on these outcomes, a probable mechanistic pathway for the production of a spiro indole-3,1'-naphthalene tetracyclic system is presented in Scheme 5. The -SO₃H group and -NH₂ groups of Sg-C₃N₄ facilitate the Knoevenagel reaction and produce isatylidene malononitrile (X) and cyclohexanone malononitrile (A). The -NH₂ group of Sg-C₃N₄ activates the cyclohexanone malononitrile and forms anion B, which attacks

the activated double bond of X with further cyclization into anion C. Subsequent intramolecular nucleophilic addition on the CN group forms an imine D. Isomerization of imine D yields the corresponding product 6.

Table 4 Recyclability experiments with Sg-C₃N₄ for various spiroindole derivatives

Cycle	Yield	Cycle	Yield
1.	96%	1.	95%
2.	96%	2.	95%
3.	96%	3.	95%
4.	96%	4.	95%
5.	95%	5.	93%
6.	95%	6.	93%



The high recyclability and the heterogeneous nature of the used $\text{Sg-C}_3\text{N}_4$ catalyst were also established (see ESI†). The results show that the $\text{Sg-C}_3\text{N}_4$ sheets are heterogeneous in nature and can be successfully reused for six cycles (Table 4).

XRD, SEM and FT-IR of the reused catalyst confirmed the analogous characteristic nature of the catalyst compared to fresh catalyst. These outcomes suggest that the morphology and structure of $\text{Sg-C}_3\text{N}_4$ sheets remain unchanged during the reaction.

3 Experimental section

A general part including instruments used is provided in the ESI.†

3.1. Synthesis of $\text{g-C}_3\text{N}_4$

Melamine (5 g) was heated at 550 °C (at a rate of 4 °C min⁻¹) using a closed crucible with a lid in a muffle furnace for 3 h. After that, the obtained material was ground into a fine powder using a mortar and pestle and referred to as $\text{g-C}_3\text{N}_4$.

3.2. Synthesis of $\text{Sg-C}_3\text{N}_4$

The as prepared $\text{g-C}_3\text{N}_4$ and 30% aqueous H_2SO_4 were placed in flask. And then it was fixed to a 12 mm tip diameter probe and the solution was sonicated at 50% power of the processor and 230 W output in a 4 s pulse mode for 4 h. The resulting mixture was poured into ice-cold water and centrifuged (12 000 rpm for 10 min twice). The obtained solid material was dried under vacuum for 24 h and referred to as $\text{Sg-C}_3\text{N}_4$.

3.3. Synthesis of spiro-pyrano chromene derivatives

A mixture of isatins (2.0 mmol), ethyl cyanoacetate/malononitrile (2.0 mmol), and 4-hydroxycoumarin (2.0 mmol) with 20 wt% $\text{Sg-C}_3\text{N}_4$ in 20 ml of water were mixed. The solution was heated under reflux conditions for an appropriate time. The progress of the conversion was monitored with TLC. After completion of the conversion the $\text{Sg-C}_3\text{N}_4$ and solid product were filtered from the solution. The precipitate was dissolved in ethyl acetate and the catalyst was recovered by centrifugation (12 000 rpm). The above residual solution was removed under reduced pressure. The final (crude) product was subjected to purification by recrystallization using ethanol.

3.4. Synthesis of a spiro indole-3,1'-naphthalene tetracyclic system

A mixture of malononitrile (4.0 mmol), isatins (2.0 mmol), and cyclic ketones (2.0 mmol) with 20 wt% $\text{Sg-C}_3\text{N}_4$ in 20 ml of water were mixed. The mixed solution was heated under reflux conditions for an appropriate time. The progress of the transformation was monitored with TLC. After completion of the transformation, $\text{Sg-C}_3\text{N}_4$ and the solid product were filtered from the solution. The precipitate was dissolved in ethyl acetate and $\text{Sg-C}_3\text{N}_4$ was recovered by centrifugation (12 000 rpm). The solvent was evaporated from the crude. And then the obtained

crude product was subjected to purification by recrystallization using ethanol.

4 Conclusions

In summary, a functionalized graphitic carbon nitride ($\text{Sg-C}_3\text{N}_4$) catalyst was prepared using an ultrasound-assisted technique and it was employed for the one-pot production of various spiro-pyrano chromenes and a spiro indole-3,1'-naphthalene tetracyclic system in aqueous media. Characterizations using different analytical tools showed that bifunctional acidic ($-\text{SO}_3\text{H}$) and basic ($-\text{NH}_2$) sites were created after functionalization. Additionally, the bifunctional nature (acidity/basicity) of the used catalyst $\text{Sg-C}_3\text{N}_4$ was confirmed *via* numerous control tests in one-pot reaction sequences. The uniqueness of this study is the simultaneous activation of the first reaction sequence by the synergistic participation of the bifunctional acidic and basic sites present in $\text{Sg-C}_3\text{N}_4$. The acidic sites present in $\text{Sg-C}_3\text{N}_4$ activated the second reaction sequence for the one-pot production of various spiro-pyrano chromenes, whereas the basic sites present in $\text{Sg-C}_3\text{N}_4$ activated the second reaction sequence for the one-pot production of a spiro indole-3,1'-naphthalene tetracyclic system. $\text{Sg-C}_3\text{N}_4$ showed no loss in activity or catalytic functionality over several runs. Diverse C-C, C-O, and C-N bonds, six-membered cycles, stereogenic centers, and spiro frameworks were designed in a single reaction.

Conflicts of interest

There are no conflicts to declare.

Acknowledgements

Financial assistance from the CSIR, UGC and DST-SERB, New Delhi is gratefully acknowledged. We are thankful to the Malaviya National Institute of Technology, Jaipur, SICART, GUJARAT and Cochin University of Science & Technology, Kochi for spectral analyses.

References

- O. C. Compton and S. T. Nguyen, *Small*, 2010, **6**, 711–723.
- K. P. Gopinath, D. V. N. Vo, D. G. Prakash, A. A. Joseph, S. Viswanathan and J. Arun, *Environ. Chem. Lett.*, 2020, 1–26.
- Y. Liu, Q. Q. Li, H. Zhang, S. P. Yu, L. Zhang and Y. Z. Yang, *N. Carbon Mater.*, 2020, **35**, 323–335.
- (a) S. S. Dang, P. Siglinda and C. Gabriele, *Chem. Rev.*, 2013, **113**, 5782–5816; (b) C. Cha, S. R. Shin, N. Annabi, M. R. Dokmeci and A. Khademhosseini, *ACS Nano*, 2013, **7**, 2891–2897; (c) A. K. Wanekaya, *Analyst*, 2011, **136**, 4383–4391; (d) K. Scida, P. W. Stege, G. Haby, G. A. Messina and C. D. García, *Anal. Chim. Acta*, 2011, **691**, 6–17; (e) L. L. Zhang and X. S. Zhao, *Chem. Soc. Rev.*, 2009, **38**, 2520–2531.
- A. K. Wanekaya, *Analyst*, 2011, **136**, 4383–4391.
- J. Zhu, P. Xiao, H. Li and S. A. Carabineiro, *ACS Appl. Mater. Interfaces*, 2014, **6**, 16449–16465.



- 7 C. Jia, L. Yang, Y. Zhang, X. Zhang, K. Xiao, J. Xu and J. Liu, *ACS Appl. Mater. Interfaces*, 2020, **12**, 53571–53591.
- 8 A. Dandia, S. L. Gupta, P. Saini, R. Sharma, S. Meena and V. Parewa, *Curr. Opin. Green Sustain. Chem.*, 2020, **3**, 100039.
- 9 (a) H. Yan, Y. Chen and S. Xu, *Int. J. Hydrogen Energy*, 2012, **37**, 125–133; (b) S. Patnaik, S. Martha, G. Madras and K. Parida, *Phys. Chem. Chem. Phys.*, 2016, **18**, 28502–28514; (c) F. Cheng, H. Wang and X. Dong, *Chem. Commun.*, 2015, **51**, 7176–7179.
- 10 G. S. Singh and Z. Y. Desta, *Chem. Rev.*, 2012, **112**, 6104–6155.
- 11 (a) J. J. Badillo, A. Silva-Garcia, B. H. Shupe, J. C. Fettinger and A. K. Franz, *Tetrahedron Lett.*, 2011, **52**, 5550; (b) S. Duce, F. Pesciaioli, L. Gramigna, L. Bernardi, A. Mazzanti, A. Ricci, G. Bartoli and G. Bencivenni, *Adv. Synth. Catal.*, 2011, **353**, 860; (c) X.-N. Wang, Y.-Y. Zhang and S. Ye, *Adv. Synth. Catal.*, 2010, **352**, 1892; (d) L.-T. Shen, P.-L. Shao and S. Ye, *Adv. Synth. Catal.*, 2011, **353**, 1943; (e) F. Zhong, X. Han, Y. Wang and Y. Lu, *Angew. Chem., Int. Ed.*, 2011, **50**, 7837; (f) N. V. Hanhan, N. R. Ball-Jones, N. T. Tran and A. K. Franz, *Angew. Chem., Int. Ed.*, 2012, **51**, 989; (g) W.-B. Chen, Z.-J. Wu, Q.-L. Pei, L.-F. Cun, X.-M. Zhang and W.-C. Yuan, *Org. Lett.*, 2010, **12**, 3132.
- 12 D. Uemura, T. Chou, T. Haino, A. Nagatsu, S. Fukuzawa, S. Z. Zheng and H. S. Chen, *J. Am. Chem. Soc.*, 1995, **117**, 1155–1156.
- 13 (a) T. H. Kang, K. Matsumoto, M. Todha, Y. Murakami, H. Takayama, M. Kitajima, N. Aimi and H. Watanabe, *Plant. Med. Phytother.*, 2002, **444**, 39; (b) O. Dideberg, J. Lamotte-Brasseur, L. Dupont, H. Campsteyn, M. Vermeire and L. Angenot, *Acta Crystallogr., Sect. B: Struct. Crystallogr. Cryst. Chem.*, 1977, **33**, 1796; (c) L. Angenot, *Plantes médicinales et phytothérapie*, 1978, **12**, 123; (d) C. H. Chou, C. L. Gong, C. C. Chao, C. H. Lin, C. Y. Kwan, C. L. Hsieh and Y. M. Leung, *J. Nat. Prod.*, 2009, **72**, 830.
- 14 A. Fomes, W. R. Adams, A. L. Adams, T. J. Berrodin, J. Cohen, C. Huselton, A. Illenberger, J. C. Karen, M. A. Hudak, A. G. Marella, E. G. Melenski, C. C. McComas, C. A. Mugford, O. D. Slayeden, M. Y. udt, J. Zhang, P. Zhang, Y. Zhu, R. C. Winneker and J. E. Wrobel, *J. Med. Chem.*, 2008, **51**, 1861.
- 15 K. Ding, Y. Lu, Z. Nikolovska-Coleska, G. Wang, S. Qiu, S. Shangary, W. Gao, D. Qin, J. Stuckey, K. Krajewski, P. P. Roller and S. Wang, *J. Med. Chem.*, 2006, **49**, 3432.
- 16 V. V. Vintonyak, K. Warburg, H. Kruse, S. Grimme, K. Hubel, D. Rauth and H. Aldmann, *Angew. Chem., Int. Ed.*, 2010, **49**, 5902.
- 17 G. Kumari, M. Modi, S. K. Gupta and R. K. Singh, *Eur. J. Med. Chem.*, 2011, **46**, 1181.
- 18 (a) M. M.-C. Lo, C. S. Newmann, S. Nagayams, E. O. Perlstein and S. L. Schreiber, *J. Am. Chem. Soc.*, 2005, **127**, 10130; (b) K. Ding, Y. Lu, Z. Nikolovska-Coleska, S. Qui, Y. Ding, W. Gao, J. Stuckey, K. Krajewski, P. P. Roller, Y. Tomita, D. A. Parrish, J. R. Deschamps and S. Wang, *J. Am. Chem. Soc.*, 2004, **126**, 16077.
- 19 (a) B. K. S. Yeung, B. Zou, M. Rottmann, S. B. Lakshminarayana, S. H. Ang, S. Y. Leong, J. Tan, J. Wong, S. Keller-Maerki, C. Fischli, A. Goh, E. K. Schmitt, P. Krastel, E. Francotte, K. Kuhen, D. Plouffe, K. Henson, T. Wagner, E. A. Winzeler, F. Petersen, R. Brun, V. Dartois, T. T. Diagana and T. H. Keller, *J. Med. Chem.*, 2010, **53**, 5155; (b) M. Rottmann, C. McNamara, B. K. S. Yeung, M. C. S. Lee, B. Zhou, B. Russell, P. Seitz, D. M. Plouffe, N. V. Dharia, J. Tan, S. B. Cohen, K. R. Spencer, G. E. Gonzalez-Paez, S. B. Lakshminarayana, A. Goh, R. Suwanarusk, T. Jegla, E. K. Schmitt, H.-P. R. Beck, F. Nosten, L. Renia, V. Dartois, T. H. Keller, D. A. Fidock, E. A. Winzeler and T. T. Diagana, *Science*, 2010, **329**, 1175; (c) S. H. Ang, P. Crastel, S. Y. Leong, L. J. Tan, W. L. J. Wong, B. K. S. Yeung and B. Zou, *US Pat.*, 2009/0275560 A1, Novartis AG, 2009; (d) Z. Zhang, Hoffmann La Roche AG spiroindolinone derivatives, PCT Int. Appl. WO 2008/055812, 2008.
- 20 T.-H. Kang, K. Matsumoto, Y. Murakami, H. Takayama, M. Kitajima, N. Aimi and H. Watanabe, *Eur. J. Pharmacol.*, 2002, **444**, 39.
- 21 (a) G. Shanthi, G. Subbulakshmi and P. T. Perumal, *Tetrahedron*, 2007, **63**, 2057–2063; (b) S. Nagaraju, B. Paplal, K. Sathish, S. Giri and D. Kashinath, *Tetrahedron Lett.*, 2017, **58**, 4200–4204; (c) S. L. Zhu, S. J. Ji and Y. Zhang, *Tetrahedron*, 2007, **63**, 9365–9372; (d) K. Jadidi, R. Ghahremanzadeh and A. Bazgir, *J. Comb. Chem.*, 2009, **11**, 341–344; (e) R. Sridhar, B. Srinivas, B. Madhav, V. P. Reddy, Y. V. D. Nageswar and K. R. Rao, *Can. J. Chem.*, 2009, **87**, 1704–1707; (f) J. Devi, S. J. Kalita and D. C. Deka, *Chemistryselect*, 2018, **3**, 1512–1516; (g) P. Das, A. Dutta, A. Bhaumik and C. Mukhopadhyay, *Green Chem.*, 2014, **16**, 1426–1435; (h) K. R. Moghadam and L. Y. T. Miri, *Tetrahedron*, 2011, **67**, 5693–5699; (i) F. Tufail, M. Saquib, S. Singh, J. Tiwari, P. Dixit, J. Singh and J. Singh, *New J. Chem.*, 2018, **42**, 17279–17290; (j) B. Karmakar, A. Nayak and J. Banerji, *Tetrahedron Lett.*, 2012, **53**, 5004–5007; (k) F. Kamali and F. Shirini, *J. Mol. Struct.*, 2021, **1227**, 129654.
- 22 (a) A. Dandia, V. Parewa, A. K. Jain and K. S. Rathore, *Green Chem.*, 2011, **13**, 2135–2145; (b) A. Dandia, V. Parewa, S. Kumari, S. Bansal and A. Sharma, *Green Chem.*, 2016, **18**, 2488–2499; (c) A. Dandia, S. L. Gupta, A. Indora, P. Saini, V. Parewa and K. S. Rathore, *Tetrahedron Lett.*, 2017, **58**, 1170–1175; (d) A. Dandia, S. Bansal, R. Sharma, D. K. Mahawar, K. S. Rathore, M. L. Meena and V. Parewa, *J. Photochem. Photobiol., A*, 2020, **389**, 112242; (e) A. Dandia, S. Khan, R. Sharma, S. Parihar and V. Parewa, *ChemistrySelect*, 2017, **2**, 9684–9690; (f) A. Dandia, S. Parihar, R. Sharma, K. S. Rathore and V. Parewa, *Nanocatalysis in green organic synthesis*, Elsevier, 2020, pp. 71–103; (g) A. Dandia, P. Saini, R. Sharma and V. Parewa, *Green organic synthesis by photochemical protocol*, Elsevier, 2020, pp. 155–198; (h) A. Dandia, R. Sharma, A. Indora and V. Parewa, *ChemistrySelect*, 2018, **3**, 8285–8290.
- 23 (a) A. Dandia, S. Parihar, P. Saini, K. S. Rathore and V. Parewa, *Catal. Lett.*, 2019, **149**, 3169–3175; (b) A. Dandia, D. K. Mahawar, R. Sharma, R. S. Badgoti, K. S. Rathore and



- V. Parewa, *Appl. Organomet. Chem.*, 2019, **33**, 5232; (c) A. Dandia, S. Bansal, R. Sharma, K. S. Rathore and V. Parewa, *RSC Adv.*, 2018, **8**, 30280–30288; (d) A. Dandia, A. Sharma, A. Indora, K. S. Rathore, A. Jain and V. Parewa, *Mol. Catal.*, 2018, **459**, 97–105.
- 24 S. Subhajyoti and R. Srivastava, *Sustainable Energy Fuels*, 2017, **1**, 1390–1404.
- 25 J. Chastain and R. C. King Jr, *Handbook of X-ray photoelectron spectroscopy*. Perkin-Elmer, USA, vol. 261, 1992.
- 26 K. Tatsuhiko, T. Toshiya, K. Takeshi, W. Yoichiro, S. Akira and F. Yoshifumi, WO2011/010715A1, 2011.
- 27 (a) T. H. Babu, A. A. Joseph, D. Muralidharan and P. T. Perumal, *Tetrahedron Lett.*, 2012, **51**, 994; (b) X.-F. Huang, Y.-F. Zhang, Z.-H. Qi, N.-K. Li, Z.-C. Geng, K. Li and X.-W. Wang, *Org. Biomol. Chem.*, 2014, **12**, 4372.

